Available online at BCREC website: https://bcrec.id

Bulletin of Chemical Reaction Engineering & Catalysis, 18 (2) 2023, 268-284

Research Article

The Effect of Variations in Calcination Temperature on the Character of ZnO and ZnO/Mopl-CTAB in Degrading Methyl Orange

Aulia Dewi Rosanti[1,*], Fahmi Hidayat[1], Yuly Kusumawati[2], Arif Fadlan[2], Rizky Arief Shobirin[1], Fanni Kurnia Wijaya[1]

[1]Department of Chemistry, Faculty of Agriculture, Universitas Islam Kadiri, Kediri 64128, Indonesia.
[2]Department of Chemistry, Faculty of Science, Institut Teknologi Sepuluh Nopember, Surabaya 60111, Indonesia.

Received: 26th May 2023; Revised: 6th July 2023; Accepted: 6th July 2023
Available online: 10th July 2023; Published regularly: August 2023

Abstract

Medan orange peel (Mopl), which has been modified using cetyltrimethylammonium bromide (CTAB), has the potential to adsorb methyl orange (MO), and thus it can be used as a supporting material for ZnO. The ZnO is a photocatalytic material that is environmentally friendly, inexpensive, non-toxic, and has a wide band gap value. This study aims to determine the effect of calcination temperature on ZnO and ZnO characteristics due to modification using Mopl-CTAB and its effect on the degradation of MO. This research was carried out by synthesizing ZnO and ZnO/Mopl-CTAB materials using impregnation method and varying the calcination temperatures at 150, 250, 350, and 450 °C. The solid material powder obtained was characterized by using Scanning Electron Microscope-Energy Dispersive X-ray (SEM-EDX), Brunauer–Emmett–Teller (BET), Fourier Transform Infra Red (FTIR), X-ray Diffraction (XRD), and Diffuse Reflectance Spectroscopy (DRS). Based on the results of the characterization, greater calcination temperature can affect the characteristics of the photocatalyst, including its morphology, functional groups, crystal structure, crystal lattice, crystallinity, surface area, pore size, pore volume, and energy band gap. The MO photodegradation activity test using the synthesized material was conducted under dark and light conditions. The results of the test revealed that the best or optimum material to be used in degrading MO is a calcined material at 450 °C under light conditions. ZnO material using Mopl-CTAB is better in degrading ZnO/Mopl-CTAB 450 °C than ZnO 450 °C. This study found that ZnO material using Mopl-CTAB had a percent removal of 78% in 50 min, while ZnO 450 °C only had a percent removal of 53% in 40 min. The reaction kinetics in dark and light conditions follow the pseudo-second-order kinetic model.

Keywords: ZnO; ZnO/Mopl-CTAB; Calcination Temperature; Methyl Orange; Photodegradation

How to Cite: A.D. Rosanti, F. Hidayat, Y. Kusumawati, A. Fadlan, R.A. Shobirin, F.K. Wijaya (2023). The Effect of Variations in Calcination Temperature on the Character of ZnO and ZnO/Mopl-CTAB in Degrading Methyl Orange. *Bulletin of Chemical Reaction Engineering & Catalysis*, 18(2), 268-284 (doi: 10.9767/bcrec.18305)

Permalink/DOI: https://doi.org/10.9767/bcrec.18305

1. Introduction

Textile industry is one of industrial sectors that has experienced rapid development in recent years. The textile industry is one of the main sectors that are welcoming Industry 4.0 [1,2]. This industrial revolution may have a positive impact on economic growth. Based on the data from the Ministry of Industry in 2019, the clothing and textile industry saw a growth of 15.08% which was the highest among other sectors. However, the increasing number of indus-

* Corresponding Author.
Email: aulia.dewi.r@uniska-kediri.ac.id (A.D. Rosanti);
Telp: +62-856-4834-6636

tries are causing environmental damage, especially in the aquatic environment [3].

Waste from the textile industry discharged directly into the aquatic environment can have physical, chemical, and biological impacts. The physical impact of textile waste contamination includes odor and color changes in polluted water environments [4]. Chemical waste may have an impact on the aquatic environment because of its hazardous materials, such as heavy metals and dangerous dyes [5]. Furthermore, biologically, textile waste contamination can disrupt the organism's life in the area around the polluted water environment [6].

Dyes commonly used in the textile industry are usually derived from azo compounds with an aromatic structure. This group of compounds is difficult to degrade naturally and can damage the environment because they are toxic, mutagenic, and carcinogenic, thus endangering biota in the environment polluted by textile waste [4–6]. Methyl orange is an azo compound that is widely found in waste from the textile industry. Rosanti *et al*. [7] successfully carried out methyl orange adsorption using modified orange peels by adding CTAB. As CTAB has cationic properties, it causes methyl orange dye to be more easily attracted by orange peel material modified by CTAB [7]. Besides adsorption, photodegradation is an effective, efficient, and inexpensive method to treat dye contamination [7,8].

Photodegradation can produce a potent oxidizing agent with high oxidizing ability, so it can degrade dyes that are difficult to degrade naturally and can be applied to both organic and inorganic compounds [4,9,10]. Many researchers have successfully degraded MO using various materials. Adeel *et al.* [11] degraded MO by precipitation method using Co-doped ZnO. One hundred mg/L MO can be degraded entirely in 130 min using 0.05 g of Co-ZnO. Chen *et al.* [12] reported that a ZnO nanomaterial catalyst synthesized via direct precipitation method could degrade MO (10 mg/L) within 120 min. Kumar *et al.* [13] showed that ZnO nano-mushrooms synthesized via solution combustion method could degrade 92% MO (10 mg/L) in 210 min. Zhou *et al.* [14] degraded MO with $ZnFe_2O_4$-SnS_2 nanocomposite, which was synthesized using solvothermal method. $ZnFe_2O_4$-SnS_2 can degrade 50 mg/L MO up to 99% in 120 min. One of photocatalysts that can be used in the photodegradation of textile waste contamination is ZnO. ZnO is chosen as a photocatalyst because it has high photocatalytic efficiency and is not toxic; therefore, it does not have the potential to contaminate the environment in its application [15–18].

Many modifications of this photocatalyst have been made to increase the activity of ZnO as a photocatalyst. Zhong *et al.* [19] synthesized modified ZnO using CTAB surfactants, producing three times better ZnO photocatalytic material than without modification with CTAB. In addition, modification of ZnO with orange peel can degrade up to 73% of methyl orange dye compared to ZnO without modification which can only degrade 34% of methyl orange in solution [8]. The variations in calcination temperature in ZnO synthesis can affect the crystal structure and energy band gap of the ZnO formed [20,21].

In this study, the synthesis of ZnO added to Medan orange peel (Mopl) and cetyltrimethylammonium bromide (CTAB) was carried out in various calcination temperatures to identify the resulting ZnO and ZnO/Mopl-CTAB characters and their ability to increase photocatalytic activity to methyl orange dye.

2. Materials and Methods

2.1 Synthesis of ZnO and ZnO/Mopl-CTAB

The synthesis method of the material was modified by Rosanti *et al*. [8]. 2 g of Medan orange peel (Mopl) was weighed, put into a beaker glass, and then added with CTAB 1%. Then 50 mL of 0.2 M zinc acetate (Merck) solution was added slowly. After that, the suspension was stirred for 30 min without heating. After 30 min, the suspension solution was heated at 60°C while being stirred, then NaOH (Merck) solution was added to pH 13 (saturated solution). The resulting suspension solution was stirred for 1 h and allowed to stand for 24 h. On the following day, the mixed solution was washed using distilled water and separated using a centrifuge at 2000 rpm for 15 min. The solid obtained was washed using acetone and dried in an oven (Memmert) at 75 °C for 8 h. The dry solids were calcined using a furnace (Thermoscientific) at various calcination temperatures of 150, 250, 350, and 450 °C. The ZnO was synthesized within the same steps without adding Mopl-CTAB.

2.2 Characterization of Synthesized Materials

The synthesized material was characterized using a Scanning Electron Microscopy (SEM) equipped with EnergyvDispersive X-ray (EDX) (Phenom Desktop ProXL) to identify the surface morphology figures and elements present on the surface of the material. Besides SEM

EDX, Brunauer–Emmett–Teller (BET) (Quantachrome Novatouch LX-4) was also used to determine surface area, pore size, and pore volume, and Fourier-transform infrared (FTIR) spectroscopy (Spectrum Two System L160000A) was used to determine functional groups present in the material. The structure, crystal system, crystallinity, crystal size, and lattice parameters were determined using X-ray diffraction (XRD) (Bruker D2 Phaser). The last characterization used diffuse reflectance spectroscopy (DRS) (Shimadzu UV – 2450) to determine the energy band gap of the synthesized material.

2.3 Photocatalytic Activity of Methyl Orange Degradation

The photocatalytic activity test of ZnO and ZnO/Mopl-CTAB at calcination temperatures of 150, 250, 350, and 450 °C was carried out by mixing 25 mL of MO with a concentration of 10 ppm with 20 mg of the material [7,22]. The solution was reacted in the photocatalytic reactor for 10, 20, 30, 40, 50, and 60 min in dark and light conditions. After the reaction was complete, the solution was separated using a centrifuge at 2000 rpm for 10 min, then the absorbance of the solution was measured using a UV-Vis spectrophotometer (T70 UV/Vis Spectrometer, PG Instruments Ltd) at 465 nm wavelength. The final concentration of the solution that has been reacted can be determined after the measurement, and the percent removal can be calculated using the following formula [8]:

$$\%Removal\ MO = \frac{[C]_0 - [C]_t}{[C]_0} \times 100\% \quad (1)$$

where, $[C]_0$ is the initial concentration of MO, and $[C]_t$ is the final concentration of MO (after the photocatalytic reaction process). Then an analysis was carried out on the kinetics of the reactions in each degradation process, both in dark and light conditions.

3. Results and Discussion

3.1 Characterization using SEM-EDX

SEM is used to determine the surface morphology of a material, while EDX is used to determine the elements and their composition on the surface of the material. Figure 1 is the surface morphology of ZnO and ZnO/Mopl-CTAB. It can be seen that the higher the calcination temperature, the more inhomogeneous the surface. Higher calcination temperatures may cause the formation of more aggregates resulting in agglomeration or clumping. However, as can be seen in Figure 1, ZnO/Mopl-CTAB with 450 °C calcination temperature treatment resulted more homogeneous than ZnO. This finding suggests that the addition of Mopl-CTAB may reduce agglomeration at high tempera-

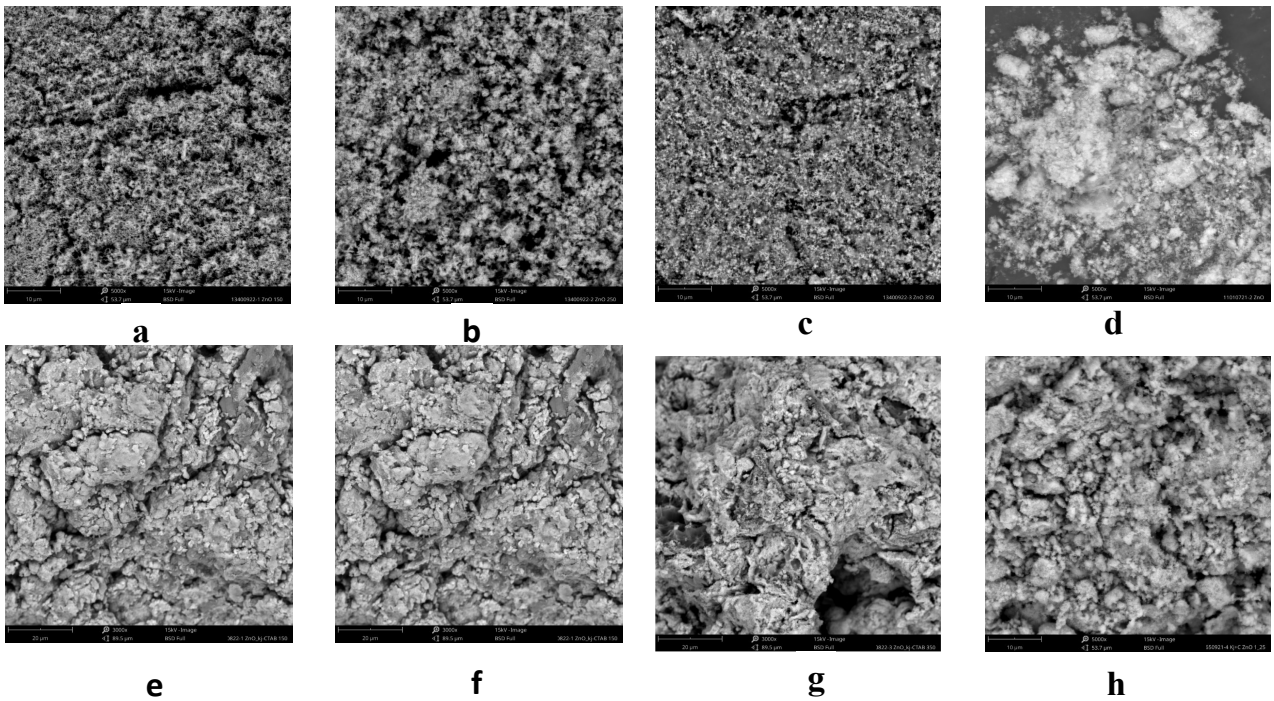

Figure 1. Surface Morphology of ZnO wurtzite with calcination temperature, (a) 150 °C, (b) 250 °C, (c) 350 °C; (d) 450 °C and ZnO/Mopl-CTAB (e) 150 °C ; (f) 250 °C; (g) 350 °C; (h) 450 °C.

tures. At low temperatures, Mopl-CTAB cannot reduce agglomeration due to the presence of CTAB. Consequently, at temperatures of 150 to 350 °C, the surface morphology of ZnO/Mopl-CTAB showed quite large and irregular aggregates. Surfactants, such as CTAB, can act as stabilizers and templates that can control size and agglomeration in crystal formation. The presence of CTAB was found to prevent the agglomeration of ZnO particles effectively [23,24].

The presence of Br in the results of elemental analysis using EDX came from the CTAB residue used as a template in the ZnO/Mopl-CTAB synthesis process. It is in line with the CTAB analysis using FTIR. The appearance of the peak at wave number 720 cm^{-1} is thought to originate from the Br from CTAB (Figure 2(a)) [25]. The presence of CTAB in ZnO/Mopl-CTAB at temperatures of 150 to 350 °C can be seen in Table 1. Table 1 shows that the presence of Br was a characteristic of CTAB compounds. It also shows that CTAB did not disappear at temperatures of 150 to 350 °C, but it disappeared at 450 °C. These findings suggest that Br evaporates at high temperatures. It was also revealed by Abdi *et al.* [26] that CTAB could completely decompose at high temperatures. Research by Bukit *et al.* [27] found that Br content in CTAB which did not go through the calcination process was only 0.15%. It shows that calcination temperatures could dramatically affect the presence of CTAB.

Based on Table 1 with respect to both ZnO and ZnO/Mopl-CTAB, the findings found that the greater the calcination temperature, the greater the percentage of Zn. It shows that the greater the calcination temperature, the more optimal the formation of ZnO can be [20].

3.2 Material Characterization using BET Surface Area

Based on Table 2, the higher the calcination temperature for both ZnO and ZnO/MOpl-CTAB, the greater the surface area of the material. Table 2 also shows that the highest surface area was the ZnO/Mopl-CTAB at a calcination temperature of 450 °C, which was greater than ZnO at a temperature of 450 °C.

Calcination of the materials at the temperature of 450 °C exhibited a dramatic increase in surface area (Table 2). The surface area of ZnO with the Mopl-CTAB modification is larger than ZnO without modification due to the loss of the CTAB component, where the CTAB can block the material's surface pores, resulting in a smaller surface area. The presence of CTAB was supported by SEM EDX data which can be seen in Table 1. Based on Table 1, at tempera-

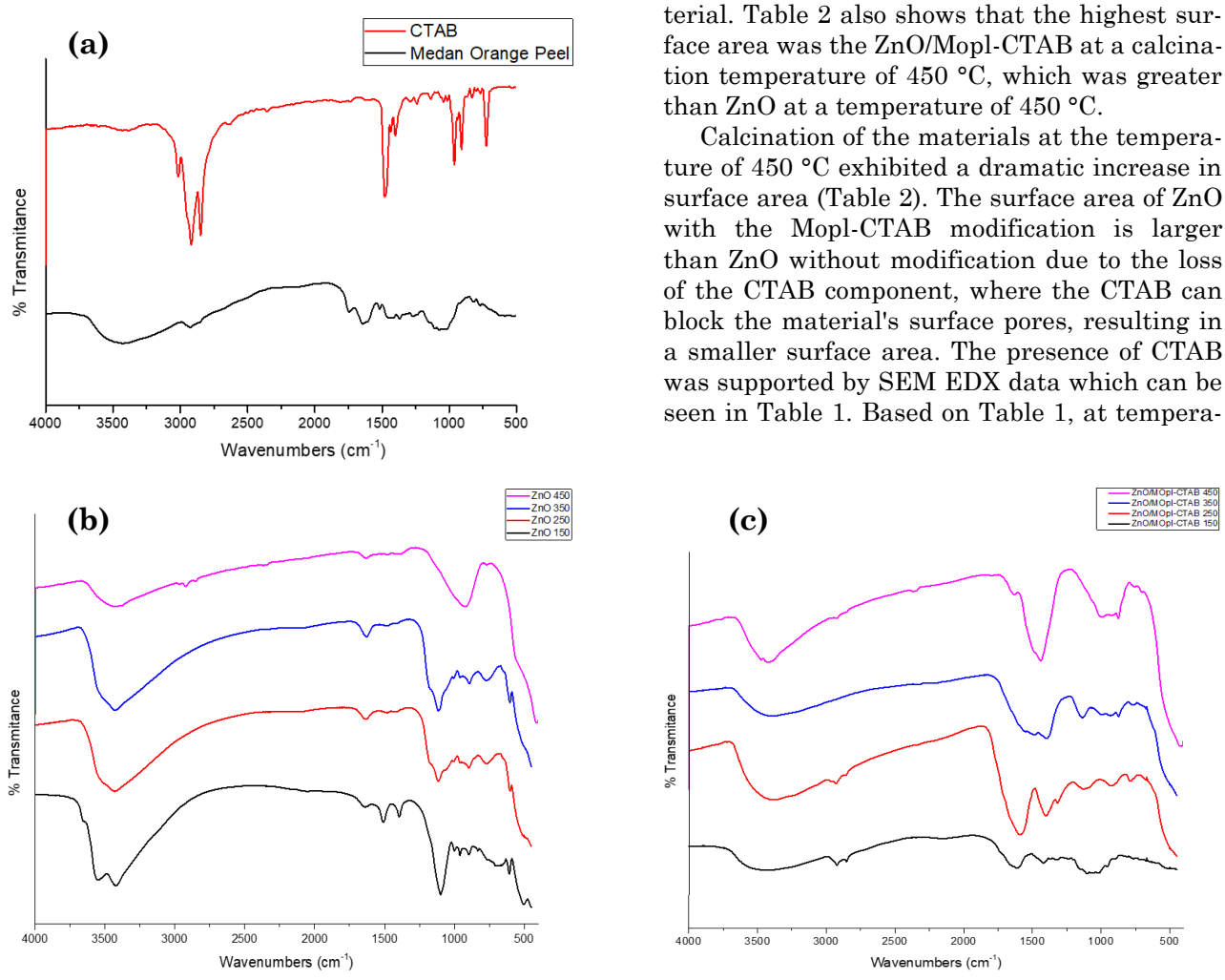

Figure 2. Spectra FTIR of (a) CTAB and Medan Orange Peel, (b) ZnO at various calcination temperatures, and (c) ZnO/Mopl-CTAB at various Calcination temperatures.

tures from 150 to 350 °C, ZnO/Mopl-CTAB material contained Br, which is a characteristic of the CTAB compound. Rosanti *et al.* [7] revealed that orange peels with the addition of CTAB has a smaller surface area because CTAB can cover the surface pores of the orange peel. At high temperatures, the CTAB will disappear leading to an increase in the surface area of the material. This suggests that CTAB could become a template or mold to obtain a larger surface area. Table 2 shows that the ZnO/Mopl-CTAB at a temperature of 450 °C had a larger surface area than that at the temperatures of 150, 250, and 350 °C whereas, at 450 °C, ZnO/Mopl-CTAB has a larger surface area than ZnO, which is equal to 36.07 m^2/ g while ZnO is only 28.08 m^2/g. Table 2 shows that higher calcination temperatures of ZnO and ZnO/Mopl-CTAB may cause a greater surface area. Higher calcination temperatures may contribute to the decomposition of the organic template and the formation of a large number of new pores during the calcination process; this may result in lower pore diameter and higher surface area [28].

The size of the pore of ZnO modified with Mopl-CTAB is larger than that of ZnO calcined at 450 °C. ZnO/Mopl-CTAB had a pore size of

Table 1. Elemental content in ZnO and ZnO/Mopl-CTAB at various calcination temperatures.

Temperature (°C)	ZnO			ZnO/Mopl-CTAB		
	Element	Atom (%)	Mass (%)	Element	Atom (%)	Mass (%)
150	Zn	35.03	69.27	O	56.32	45.73
	O	52.51	25.41	Si	14.05	28.57
	C	10.82	3.93	C	26.76	16.31
	Si	1.64	1.39	Zn	2.8	9.29
				Br	0.07	0.1
250	Zn	38.1	70.9	Zn	16.47	48.08
	O	54.48	24.81	O	37.58	26.85
	C	6.54	3.59	C	45.54	24.43
	Si	0.88	0.7	Si	0.35	0.44
				Br	0.06	0.21
350	Zn	45.81	77.85	Zn	36.69	71.79
	O	46.29	19.25	O	35.54	17.02
	C	6.87	2.14	C	26.27	9.44
	Si	1.03	0.75	Ca	1.03	1.24
				Si	0.39	0.33
				Br	0.07	0.18
450	Zn	47.43	77.98	Zn	39.9	73.26
	O	42.79	17.22	O	52.03	23.38
	S	2.9	2.34	C	6.65	2.24
	C	5.92	1.79	Si	1.42	1.12
	Si	0.96	0.68			

Table 2. Surface Area, Pore Size and Pore Volume of ZnO and ZnO/Mopl-CTAB at various calcination temperatures.

Material	Temperature (°C)	Surface Area (m^2/g)	Pore size (nm)	Pore volume (cm^3/g)
ZnO	150	10.75	3.93	2.12×10^{-2}
	250	20.14	6.10	6.14×10^{-2}
	350	22.66	4.20	4.76×10^{-2}
	450	28.08	3.90	5.81×10^{-2}
ZnO/Mopl-CTAB	150	0.415	3.87	0.08×10^{-2}
	250	0.457	10.22	0.23×10^{-2}
	350	23.87	4.47	5.34×10^{-2}
	450	36.07	4.63	8.34×10^{-2}

4.63 nm, while ZnO was only 3.93 nm. These findings suggest that CTAB only increases the pore diameter distribution of the material. It causes CTAB to only act as a template or mold to increase the size of the pore of CTAB [29]. In Table 2, it can be seen that given the size of the pore, all materials can be classified as mesoporous materials with the pore size in the range of 2-50 nm [30,31]. The advantage of mesoporous materials is that they have a larger surface area than microporous materials, thus allowing for a more comprehensive contact binding site between the adsorbate and adsorbent [32].

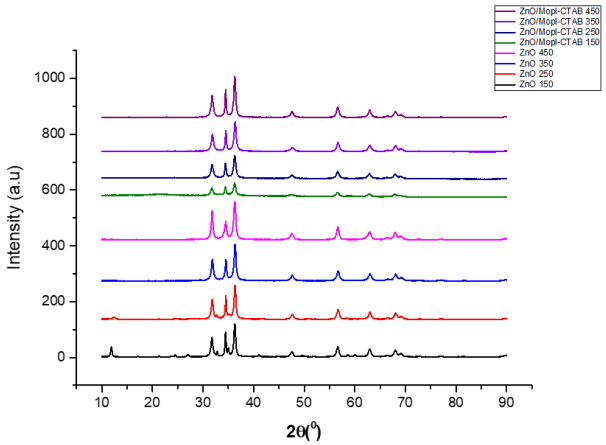

Figure 3. XRD diffractogram of bare ZnO and ZnO/Mopl-CTAB materials with variations in calcination temperature.

3.3 FTIR Characteristics

FTIR measurements determine the proper calcination temperature in forming ZnO/Mopl-CTAB materials. Figure 2(a) is the FTIR spectra of CTAB and orange peel. Weak signals in the 3015 cm^{-1} region were identified as C–CH_3 asymmetric stretching vibrations and N–CH_3 symmetric stretching vibrations of CTAB. The FTIR spectra of CTAB showed two strong bands, stretching vibrations of the asymmetric C–CH_2 bond at wave number 2918 cm^{-1} and symmetrical at 2848 cm^{-1} in the methylene chain. The sharp bands at wave numbers between 1400-1500 cm^{-1} are the deformation of the $-CH_2-$ and $-CH_3$ groups of the long carbon chains in CTAB. The band at 720 cm^{-1} could be assigned to Br^- [25,33–35].

Meanwhile, in the orange peel FTIR spectra, it can be seen that high absorption at about 3400 cm^{-1} corresponds to OH stretching vibrations of phenols and alcohols. The peak at 2926 cm^{-1} corresponds to the CH stretch vibrations in lignin, cellulose, and hemicellulose. The peak around 1743 cm^{-1} is due to unconjugated C=O groups, while conjugated C=O ab-

Table 3. Diffractogram data of ZnO wurtzite crystals with variations in calcination temperature.

(*hkl*)	150 °C			250 °C			350 °C			450 °C		
	2θ (°)	I_C	I_T	2θ (°)	I_C	I_T	2θ (°)	I_C	I_T	2θ (°)	I_C	I_T
Bare ZnO												
(100)	31.75	47.78	51.25	31.82	47.88	50.24	31.85	55.43	59.46	31.80	60.42	63.90
(002)	34.45	33.73	39.59	34.52	31.34	36.48	34.53	34.28	39.88	34.46	45.00	49.74
(101)	36.27	73.35	83.28	36.32	78.20	86.80	36.33	86.97	94.50	36.27	109.38	118.61
(102)	47.56	15.52	18.70	47.64	16.71	18.94	47.65	18.49	20.26	47.57	26.87	28.83
(110)	56.63	31.23	33.06	56.69	31.85	33.37	56.70	33.51	35.28	56.64	38.03	40.31
(103)	62.94	23.44	26.20	63.00	22.47	24.74	63.00	26.02	28.42	62.89	33.54	36.45
(200)	66.49	6.02	8.15	66.56	6.64	9.64	66.55	5.83	8.05	66.46	6.90	9.18
(112)	68.03	25.49	28.48	68.10	23.63	26.26	68.10	24.06	26.61	68.01	28.84	31.89
(201)	69.04	21.82	23.89	69.15	13.96	15.61	69.14	18.13	20.10	69.09	18.10	19.25
ZnO/Mopl-CTAB												
(100)	31.77	22.40	30.75	31.79	37.62	42.38	31.87	45.52	49.14	31.80	60.08	63.42
(002)	34.42	14.61	24.09	34.44	26.09	34.96	34.51	29.79	33.55	34.47	37.63	42.09
(101)	36.24	34.02	44.22	36.27	65.24	73.63	36.34	77.80	84.58	36.28	98.53	104.12
(102)	47.52	13.59	18.86	47.56	13.76	17.97	47.63	17.83	20.25	47.60	21.04	24.62
(110)	56.58	28.00	32.46	56.62	25.44	28.34	56.69	32.40	33.95	56.63	33.71	35.51
(103)	62.84	22.42	26.21	62.89	22.72	25.54	62.95	25.94	28.22	62.94	25.18	27.38
(200)	66.42	6.13	10.31	66.48	6.61	9.85	66.55	6.39	9.29	66.49	6.02	8.81
(112)	67.96	21.74	25.66	68.00	23.59	27.16	68.06	23.52	27.82	68.03	24.46	27.49
(201)	68.99	17.60	20.53	69.01	15.73	17.59	69.11	17.74	19.95	69.07	15.50	17.61

I_C = Intensities of Crystalline Phase; I_T = Total Intensities (Amorphous and Crystalline Phase)

sorbs at a lower wavelength (about 1645 cm^{-1}). Bands between 1300 and 1000 cm^{-1} are assigned to CO groups present in lignin and polysaccharides [7,36,37].

Figure 2(b) is the spectra of the ZnO material, which has been calcined at various temperatures. The wide vibrational band between 400 and 600 cm^{-1} on all spectra could be assigned as a metal-oxygen (Zn−O) stretching vibration [38]. The broadband about 3500 cm^{-1} is assigned to O−H stretching (hydroxyl group) that signifies the hygroscopic of ZnO. Minor bands between 600 and 1000 cm^{-1} denote the Zn−OH bond due to the presence of the $Zn(OH)_2$ group. It is still present during the ZnO formation process, which disappears with increasing calcination temperature [39,40].

During the calcination process of ZnO/Mopl-CTAB under 450°C (Figure 2(c)), residue from orange peel and CTAB peaks were still observed. These bands are still clearly visible in the 150°C calcination process and disappear with increasing calcination temperature [18]. The higher the calcination temperature, the sharper the peak intensity of the ZnO material and the higher the percentage of ZnO. It is shown by the elemental analysis in the EDX SEM that detected higher percentages of Zn and oxygen (Table 1).

3.4 XRD Characteristics

ZnO and ZnO/Mopl-CTAB with treatment temperatures of 150-450°C had the same dominant crystal structure. It is ZnO wurtzite structure (JCPDS 36-1451 and ICDD 4-5-4711) showing a similar diffraction pattern (Figure 3) at an angle diffraction range of 31° (100), 34° (002), 36° (101), 47° (102), 56° (110), 62° (103), 66° (200), 68° (112), and 69° (201), as shown in Table 3 [41]. The similarity in hexagonal wurtzite crystal structure between ZnO and ZnO/Mopl-CTAB showed no significant change in ZnO crystal structure. ZnO crystals without and with the addition of Mopl-CTAB still have the characteristics of the P63mc space group (186). Although bare ZnO was heated at low-temperature, the crystals still contained hydrozincite $Zn_5(OH)_6(CO_3)_2$ with space group $C2m$ (12). It was confirmed at a prominent diffraction angle (Table 4) in the range of 12° (200), 24° (310), 32° (021), 35° (221), 41° (40-2), 50° (33-1), 58° (040), 60° (023), and 77° (623) according to ICDD 4-13-7572 [41]. Thus, these findings have demonstrated that the process of forming ZnO wurtzite crystals begins with the decomposition of Zn-acetate to hydrozincite. Then with further heating, the hydrozincite will further decompose and rearrange the crystals to be ZnO wurtzite (Figure 5) [42]. On the other hand, the addition of Mopl-CTAB could

Table 4. Diffractogram Data Finding of $Zn_5(OH)_6(CO_3)_2$ Hydrozincite Crystals at a calcination temperature of 150-250 °C.

Bare ZnO												
(*hkl*)	150 °C						250 °C					
	2θ (°)	I_C	I_T	β (°)	*%Cryst*	*L* (nm)	2θ (°)	I_C	I_T	β (°)	*%Cryst*	*L* (nm)
(200)	11.88	47.78	51.25	0.69	91.70	11.65	12.41	6.82	1.73	1.13	79.80	7.07
(001)	17.09	33.73	39.59	0.58	78.34	13.95						
(11-1)	21.30	73.35	83.28	0.34	68.88	23.62						
(111)	24.02	15.52	18.70	1.77	75.74	4.60						
(310)	24.48	31.23	33.06	0.61	67.41	13.41	24.80	3.47	2.84	1.72	54.95	4.74
(31-1)	27.00	23.44	26.20	1.21	80.30	6.75						
(021)	32.80	6.02	8.15	0.47	66.06	17.51	32.73	7.12	4.22	0.80	62.80	10.35
(221)	35.01	25.49	28.48	0.59	82.06	14.01	35.12	7.63	1.95	1.19	79.68	7.02
(40-2)	41.04	21.82	23.89	0.81	74.90	10.50	41.63	1.96	1.16	1.62	62.89	5.26
(33-1)	49.73	47.78	51.25	2.74	78.36	3.19	50.85	2.77	1.93	2.02	58.85	4.35
(62-1)	51.88	33.73	39.59	0.99	51.40	8.89						
(040)	58.61	73.35	83.28	0.68	64.08	13.47	58.45	2.36	2.16	0.82	52.18	11.06
(023)	60.05	15.52	18.70	0.56	68.17	16.25	60.21	0.98	1.17	1.18	45.55	7.75
(821)	66.50	31.23	33.06	2.08	79.67	4.56						
(24-2)	70.10	23.44	26.20	0.93	51.71	10.47						
(623)	77.05	6.02	8.15	1.62	67.36	6.27	77.09	3.49	2.31	1.78	60.19	5.70
Average Value					71.63	11.19					61.88	7.03

I_C = Intensities of Crystalline Phase; I_T = Total Intensities (Amorphous and Crystalline Phase)

significantly help bind acetate ions, thereby reducing the possibility of Zn-acetate decomposition into hydrozincite. As a result, Zn-acetate could be directly decomposed into ZnO wurtzite.

3.4.1 Lattice parameters and degree of crystallinity

The shape of the diffraction peaks also represents the degree of crystallinity and the size of the crystallites. The sharper and narrower the shape of the diffraction peaks with a lower peak base, the larger the crystallite size with a high degree of crystallinity. Using XRD data, the distance between lattice planes (*d*) can be calculated using Bragg's law [43]. From the diffraction data, the degree of crystallinity (*%Cryst*) can also be determined from the intensity data obtained at each peak [*hkl*]. In addition, it can be used to further determine lattice parameters with the assumption that there are two-phase crystal systems: hexagonal ZnO wurtzite and monoclinic hydrozincite[44]. The crystallinity percentage of each ZnO wurtzite lattice for each sample at 150-450 °C can be seen in Figure 4.

The distance between *d* lattice planes can be related to the lattice parameters *a*, *b*, and *c* for the hexagonal crystal system. As for the monoclinic crystal system, the distance between lattice plane *d* could be used to determine lattice parameters *a*, *b*, and *c* with lattice angle *β* [43].

The results of the XRD characterization of ZnO wurtzite crystals are presented in Table 3, and those of hydrozincite crystals are in Table 4. Meanwhile, the results of the lattice parameter calculation and the degree of crystallinity of ZnO wurtzite and ZnO hydrozincite are presented in Table 5 and Figure 4. The crystallographic interpretation of XRD data used Crystal Sleuth software, while the crystal structure representation used VESTA [41,45].

The addition of Mopl-CTAB to ZnO had an impact on the degree of crystallinity and crystallite size, as shown in Figure 4 and Table 5. Mopl and CTAB added to ZnO caused the degree of crystallinity of ZnO/Mopl-CTAB to be lower than that of ZnO. This decrease showed that Mopl-CTAB intervened in the growth of ZnO crystals, and consequently the growth of ZnO crystals added with Mopl-CTAB was inhibited. Table 5 shows the effect of adding Mopl-CTAB to ZnO on the change of the lattice parameters of ZnO. At the beginning of heating, the temperatures of 150-250 °C caused a narrowing of the hydrozincite lattice that would decompose and transform into ZnO wurtzite. At the same time, lattices a and b and c of ZnO in both bare ZnO and ZnO/Mopl-CTAB were compressed. The compression contributed to the formation of ZnO wurtzite crystals resulting from the decomposition of Zn-acetate (in bare ZnO and ZnO/Mopl-CTAB) as

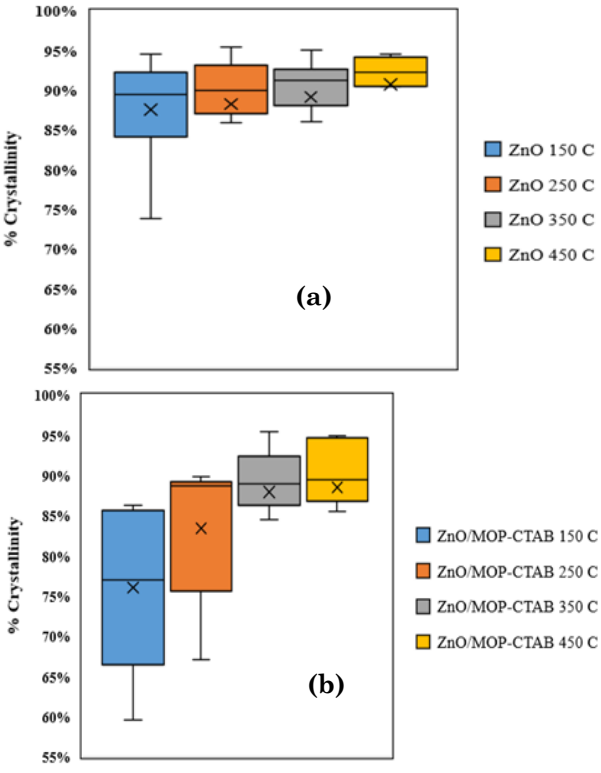

Figure 4. The degree of crystallinity of ZnO wurtzite at (a) bare ZnO, and (b) ZnO/Mopl-CTAB with a calcination temperature of 150-450 °C.

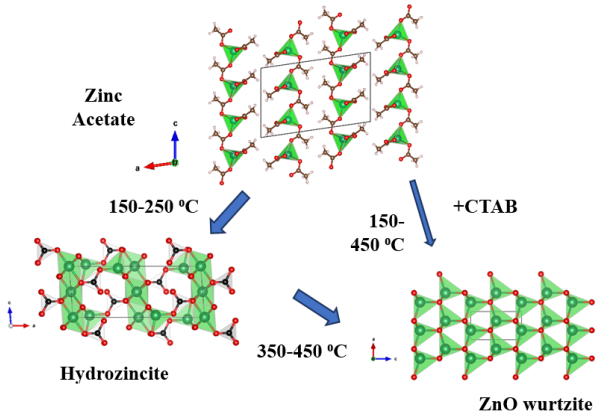

Figure 5. Schematic illustration of transformation of Zn-acetate is partially decomposed into $Zn_5(OH)_6(CO_3)_2$ hydrozincite crystals, then further decomposed into. The addition of CTAB helps the decomposition of Zn-acetate into ZnO wurtzite without being terminated into hydrozincite first.

well as decomposition and hydrozincite transformation (at bare ZnO).

Furthermore, a temperature change from 250 °C to 450 °C was responsible for expanding the lattice of ZnO wurtzite crystals in bare ZnO. On the other hand, adding Mopl-CTAB to ZnO gave different transformation phenomena that experienced lattice compression. When CTAB decomposed at temperatures of 350-450 °C, ZnO was compressed and rearranged the atomic structure in ZnO wurtzite crystals, as confirmed in the downward trend of the lattice in Table 5, in which lattices *a*, *b*, and *c* were compressed.

3.4.2 Crystallite size and Strain Estimation

Crystallographic interpretation is carried out to extract information, such as full weight at half maximum (FWHM), that would later be used to determine crystallite size. The calculation method used the Debye-Scherrer equation by considering the peak width to calculate crystallite size in a specific lattice plane (L_{hkl}) [46]. The method for calculating crystallite size was then developed. This was done by considering the broadening of the diffraction peaks influenced by the crystallite size and strain; therefore, the average crystallite size and strain is determined using the Williamson-Hall plot [47]. After determining the linear regression equation, the slope can be determined to obtain ε as the crystallite strain, as well as the y-intercept to obtain L as a representative of the crystallite size (nm). The results of the crystal-

Table 5. Crystal Lattice Parameters of ZnO wurtzite and hydrozincite obtained from bare ZnO and ZnO/Mopl-CTAB with variations in calcination temperature.

	ZnO				ZnO/Mopl-CTAB			
	150 °C	250 °C	350 °C	450 °C	150 °C	250 °C	350 °C	450 °C
Crystal Structure	ZnO Wurtzite							
Crystal System	Hexagonal							
Space Group (no.)	P63mc (186)							
%Crystalinity	87.56	87.56	87.56	87.56	76.02	76.02	76.02	76.02
$a = b$ (Å)	3.247	3.246	3.247	3.251	3.251	3.25	3.249	3.249
c (Å)	5.198	5.197	5.2	5.2069	5.209	5.206	5.207	5.201
$\alpha = \beta$ (°)	90	90	90	90	90	90	90	90
γ (°)	120	120	120	120	120	120	120	120
Crystal Structure	$Zn_5(OH)_6(CO_3)_2$ - hydrozincite							
Crystal System	Monoclinic							
Space Group (no.)	C2m (12)							
a (Å)	13.41	13.2						
b (Å)	6.25	6.22						
c (Å)	5.29	5.26						
$\alpha = \gamma$ (°)	90	90						
β (°)	94.4	93.2						

Table 6. Crystallite size of ZnO wurtzite from bare ZnO and ZnO/Mopl-CTAB with variations in calcination temperature.

ZnO				
T (°C)	150 °C	250 °C	350 °C	450 °C
Slope	0.04301599	0.04553296	0.04454819	0.04251011
Intercept	0.00404908	0.00314300	0.00187000	0.00107265
Crystallite Size/ L (nm)	34.2424452	44.1140312	74.1445989	129.2596840
Strain/ ε	0.01075400	0.04553296	0.01113705	0.01062753
ZnO/Mopl-CTAB				
T (°C)	150 °C	250 °C	350 °C	450 °C
Slope	0.04445359	0.04643979	0.04445359	0.04072871
Intercept	0.00301805	0.00460792	0.00301805	0.00282485
Crystallite Size/ L (nm)	45.9403920	30.0895849	45.9403920	49.0823938
Strain/ ε	0.01111340	0.01160995	0.01111340	0.01018218

lite size calculation using the Debye-Scherrer equation are presented in Figure 6.

The addition of Mopl-CTAB changed the crystallite size and strain in ZnO crystals. From the plot data presented in Figure 6 and Table 6, the addition of Mopl-CTAB decreased the ZnO crystallite size when compared to ZnO without any additions. In the results of the Williamson-Hall plot, adding Mopl-CTAB reduced crystallite size slightly and marginally increased crystallite strain. Generally, the size of ZnO wurtzite crystals was found to increase with the increase in calcination temperature. The difference between bare ZnO and ZnO with the addition of Mopl-CTAB was that the crystal growth rate in bare ZnO crystal signifi-

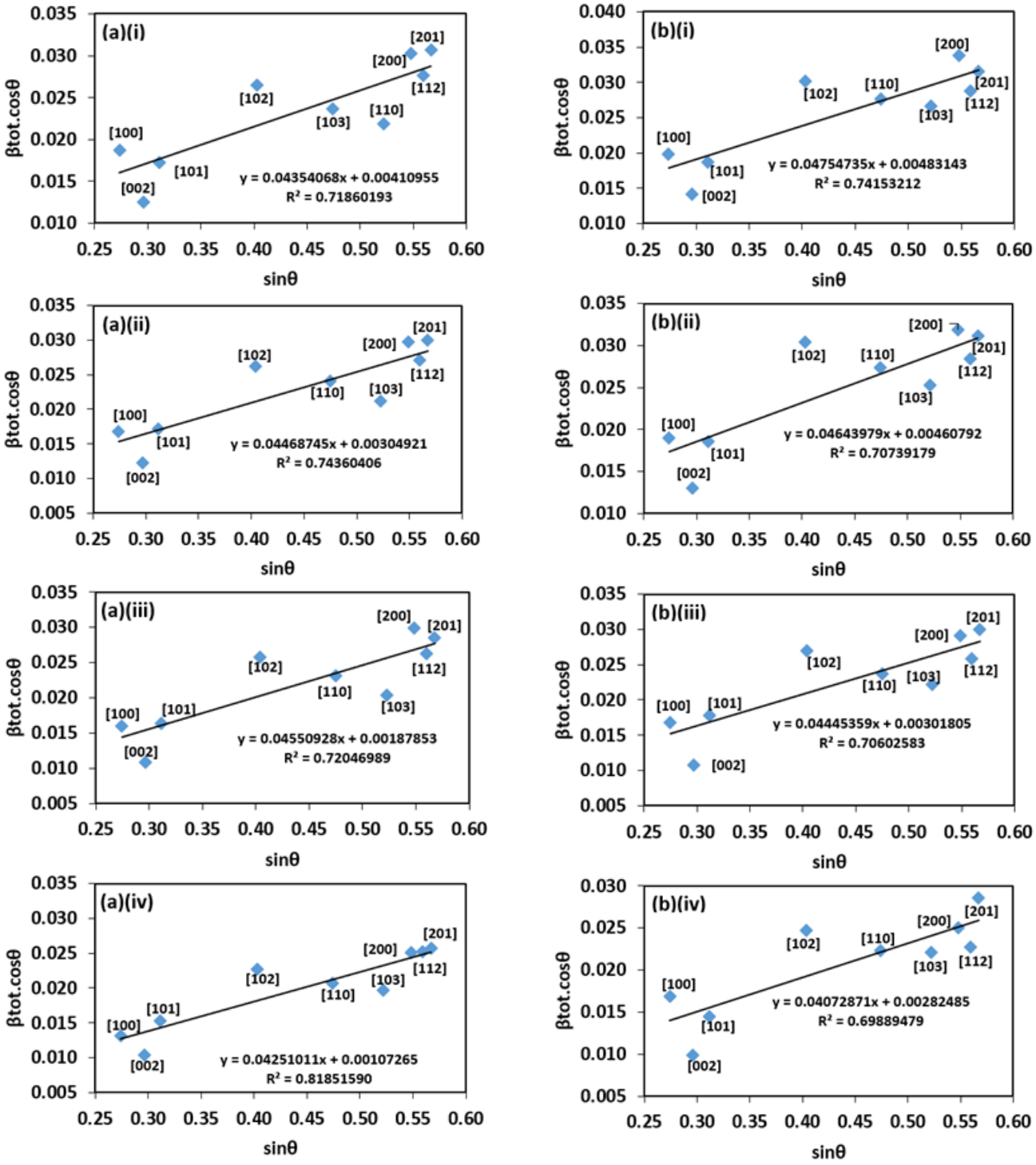

Figure 6. Size-strain Data Plot with Williamson-Hall Method Approach of ZnO extracted from (a) bare ZnO, and (b) ZnO/Mopl-CTAB; the materials were calcined in various temperatures, (i) 150 °C, (ii) 250 °C, (iii) 350 °C, and (iv) 450 °C.

cantly increased compared to that of ZnO with the addition of Mopl-CTAB. The decrease in crystallite size shows that Mopl-CTAB may contribute to ZnO crystal defects. Furthermore, Mopl-CTAB may cause ZnO crystals as ZnO/Mopl-CTAB to grow less freely. This may decrease the crystallite size, as confirmed by SEM photography (Figure 1) which shows that the crystallite size of the ZnO/Mopl-CTAB was smaller and more evenly distributed than ZnO.

3.5 Effect of Temperature on Energy Band Gap Values

Energy band gap can be determined by using DR-UV analysis. DR UV analysis is carried out at wavelengths in the range of 200-900 nm, then the %R (reflectance) value is obtained then entered into the Tauc equation [48]. Band gap values can affect the photocatalytic performance of semiconductor materials. The findings of this study suggest that the greater the calcination temperature, the smaller the resulting band gap value. Table 7 shows that ZnO/Mopl-CTAB at 450 °C has the smallest E_g value with 3.157, while the E_g value of ZnO 450 is only 3.272 eV. The band gap value was inversely proportional to the edge absorption (λ_{edge}). The smaller the E_g value, the greater the edge absorption. Greater edge absorption value shows that the material is responsive to visible light whose wavelengths cover a range above 400-800 nm [7].

Based on Table 7, ZnO/Mopl-CTAB with a calcination temperature of 450 °C had the most significant absorption at the edge, which was 393.174 nm. However, the absorption value at the edge was still below the visible light range, suggesting that with greater calcination temperature, the absorption at the edge may increase the shift to the right or towards the visible light region.

3.6 Degradation Activity Test of MO using ZnO and ZnO/Mopl-CTAB at Various Calcination Temperatures

The application of the composite material to degrade MO was carried out in both dark and light conditions. Figure 7 shows the use of ZnO material in dark and light conditions. The greater the calcination temperature, the greater the percent removal of color that occurs in dark and light conditions. In the dark, it can be seen that the optimum percent removal which occurred at 40 min using ZnO 450 °C was 41%. In light conditions, it was 54% at 30 min using ZnO 450 °C. The results of this study may suggest that the greater the calcination temperature, the greater the percent removal. It is because the more significant the calcination temperature, the better the ZnO crystal formation, as indicated by the energy band gap value of ZnO in Table 7. Table 7 shows that the higher the calcination temperature, the smaller the

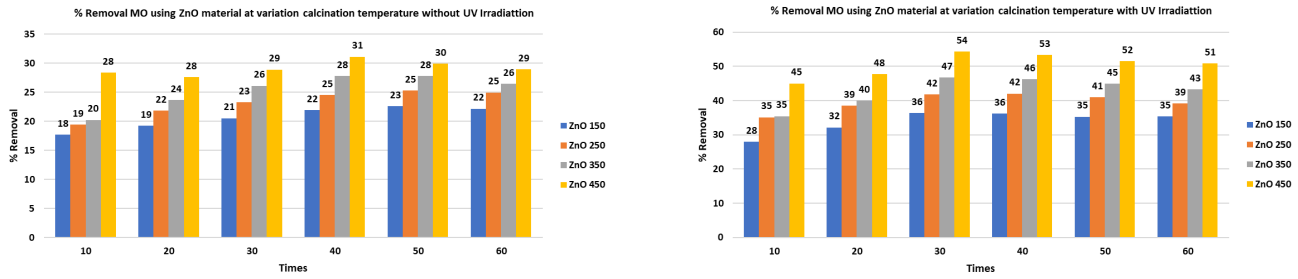

Figure 7. %MO removal by ZnO with variations in calcination temperature in the absence of UV irradiation or dark conditions (DC) and with UV irradiation or bright conditions (LC).

Table 7. Bandgap energy values of ZnO and ZnO/Mopl-CTAB with variations in calcination temperature.

Materials	Temperature (°C)	E_g	λ_{tepi} (nm)
ZnO	150	3.378	367.451
	250	3.321	373.758
	350	3.315	374.434
	450	3.272	379.355
ZnO/Mopl-CTAB	150	3.351	370.412
	250	3.318	374.096
	350	3.294	376.821
	450	3.157	393.174

band gap value. As the band gap value decreases, it will further enhance the photodegradation process. The smaller the band gap value, the greater the edge absorption. This may indicate that the material is more responsive to visible light with wavelengths in the range above 400-800 nm, and thus percent MO removal using ZnO in light conditions is more significant than in the dark. In light conditions, the photocatalytic process is more optimal because there is light, while in dark conditions, the process is not optimal because there is no light.

This result is also supported by the results of the SEM characterization, where the greater the calcination temperature, the greater the Zn element produced. The greater the Zn element, the more optimal the photocatalytic process. The photodegradation activity test was carried out in dark and light conditions to separate the adsorption reaction from the photocatalytic reaction to ensure that the reaction was a photodegradation reaction. From Figure 8, it can be seen that the catalytic activity in dark and light conditions is contradictory because the photocatalytic process may not occur in the dark. Furthermore, there is no light source to perform the degradation reaction. Under light conditions, a photocatalytic process could occur because light helps the photocatalytic reaction. In the photocatalytic reaction, the band gap value affects the reaction process significantly. Table 7 shows that the material with a calcination temperature of 450 °C has a smaller band gap value than the others and shows the best photocatalytic reaction.

The use of ZnO/Mopl-CTAB materials at various calcination temperatures in degrading MO can be seen in Figure 8. Comparison of Figure 7 and Figure 8 shows that the use of ZnO/Mopl-CTAB materials is better at degrading MO than ZnO. Because ZnO/Mopl-CTAB has a smaller energy band gap value than ZnO (Table 7), the use of ZnO material modified with Mopl-CTAB is more optimal than ZnO without modification. A smaller band gap value allows the photocatalytic material to absorb photons more easily, causing the photodegradation process to increase.

In contrast to ZnO, the best dark condition of the material is ZnO/Mopl-CTAB with a 150 °C calcination temperature which is 52% at 50 min. In light conditions, the most optimum percent removal was ZnO/Mopl-CTAB 450 °C with 78% at 50 min. Based on Figure 8, the ZnO/Mopl-CTAB material in the dark conditions shows that the higher the calcination temperature, the lower the percent removal. It is because of the presence of CTAB in the ZnO/Mopl-CTAB material at temperatures from 150 °C to 350 °C. MO is an anionic dye, and CTAB has cationic properties, which may cause anionic dyes to be attracted more efficiently [7]. These CTAB properties cause ZnO/Mopl-CTAB with a temperature of 450 °C has the greatest % removal because of in the dark conditions, only adsorption processes occur, and no photocatalytic processes.

In contrast, in light conditions, the higher the calcination temperature, the greater the percent removal produced. It is because higher calcination temperatures may cause the CTAB to disappear to increase the surface area of the ZnO material, as shown in the characteristics using BET in Table 2. The increased surface area of this material shows that CTAB is only a mold. Thus, no trace of CTAB at high temperatures could result in a larger surface area and prevent agglomeration as displayed in Figure SEM (Figure 1). It has been suggested that ZnO/Mopl-CTAB 450 °C has morphology with less agglomeration than ZnO 450 °C.

3.7 Kinetics of the Photodegradation Reaction of MO using ZnO and ZnO/Mopl-CTAB at Various Calcination Temperatures

The reaction kinetics of the photodegradation process of MO with ZnO and ZnO/Mopl-CTAB at various calcination temperatures were determined using an equation model of the pseudo-first-order and pseudo-second-order reactions. In the kinetics of the reaction, the

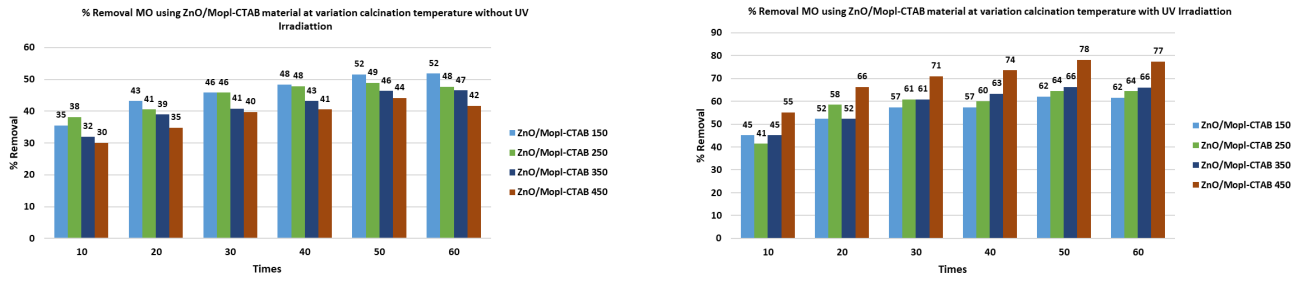

Figure 8. %MO removal by ZnO and ZnO/Mopl-CTAB with variations in calcination temperature in the absence of UV irradiation or dark conditions (DC).

pseudo-first-order model is obtained based on the existence of a mass balance that assumes the rate between the dyes that are successfully adsorbed or degraded and the reaction time that is proportional to the dyes absorbed at various times (q_e–q_t). The reaction kinetics of the pseudo-first-order model can be formulated by Eq. (2) [7]:

$$\ln\left(q_e - q_t\right) = \ln q_e - k_1 t \quad (2)$$

$$\frac{t}{q_t} = \frac{1}{k_2 q_e^2} + \frac{1}{q_e} t \quad (3)$$

where, q_e = MO concentration at equilibrium; q_t = MO concentration at time t; t = contact time (min); k_1 is the reaction rate constant. When t=0, then q_t=0, and when t=t, then q_t=q_t. The reaction rate constant could be determined by plotting the intermediate graph by making a graph with the y-axis and time (t) on the x-axis. The pseudo-second-order model of adsorption kinetics or pseudo-chemical reaction can be described in Eq. (3) where the reaction rate constant or k_2 can be determined by plotting a graph between t/q_t as the y-axis and time (t) as the x-axis. Figure 9 displays the graph of the reaction kinetic model of MO with ZnO and ZnO/Mopl-CTAB in dark and light conditions, while Table 8 shows the value of the reaction rate constant and the regression value of R^2 as well as each reaction kinetic model.

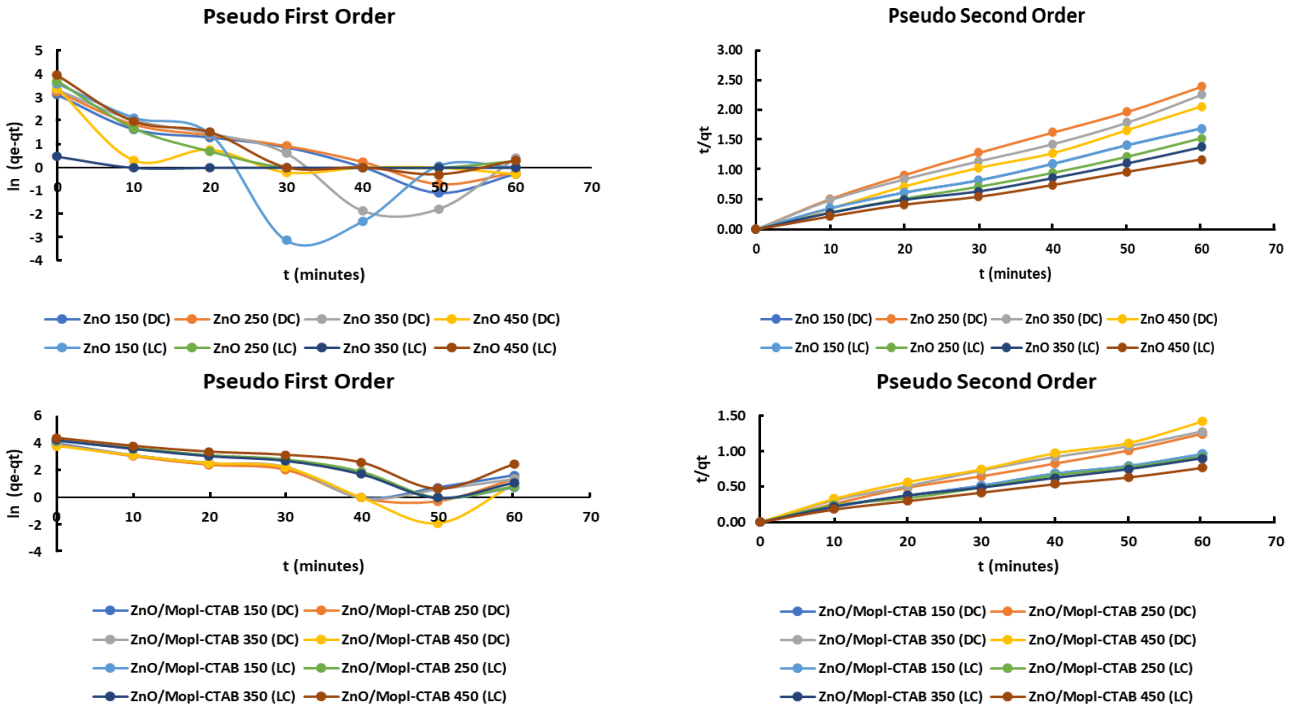

Figure 9. First-order and pseudo-second-order pseudo-kinetic models of all reactions in light and dark conditions.

Table 8. The value of reaction rate constants in methyl orange photodegradation reactions using ZnO and ZnO/Mopl-CTAB at various calcinations temperature in dark and light condition.

Sample	Without UV Irradiation Condition				With UV Irradiation Condition			
	Pseudo First Order		Pseudo Second Order		Pseudo First Order		Pseudo Second Order	
	k_1	R^2	k_2	R^2	k_1	R^2	k_2	R^2
ZnO150°C +MO	0.0609	0.8770	0.0043	0.9958	0.0665	0.3619	0.0041	0.9966
ZnO250°C +MO	0.0594	0.9078	0.0054	0.9962	0.0512	0.6465	0.0043	0.9963
ZnO350°C +MO	0.0706	0.6334	0.0060	0.9936	0.0052	0.375	0.0050	0.9977
ZnO450°C +MO	0.0445	0.5487	0.0095	0.9970	0.0610	0.7335	0.0057	0.9967
ZnO/Mopl-CTAB150°C +MO	0.0509	0.6480	0.0202	0.9915	0.0665	0.8969	0.0206	0.9938
ZnO/Mopl-CTAB250°C +MO	0.0592	0.7001	0.0181	0.9953	0.0699	0.8891	0.0368	0.9917
ZnO/Mopl-CTAB350°C +MO	0.0537	0.7038	0.0176	0.9910	0.0639	0.8656	0.0822	0.9906
ZnO/Mopl-CTAB450°C +MO	0.0750	0.6732	0.0930	0.9904	0.0459	0.6875	0.1849	0.9938

As discussed earlier, all MO degradation reactions in dark and light conditions follow the pseudo-second-order model because the value of the regression results or R^2 in the pseudo-second-order model is close to 1. In the case of the value of the reaction rate in light conditions, the greater the calcination temperature, the higher the reaction rate. It is indicated by the increasing value of k_2 as the calcination temperature rises. In addition, in light conditions, the value of the reaction rate constant of all ZnO/Mopl-CTAB materials is greater than that of ZnO.

In contrast, as regards ZnO/Mopl-CTAB under dark conditions, the higher the calcination temperature, the slower the reaction rate because of the presence of CTAB. In dark conditions, an increase in the calcination temperature can lead to the loss of CTAB and lower values of the reaction rate constant in the ZnO/Mopl-CTAB. It shows that in dark conditions, the reaction is an adsorption reaction, while in light conditions, it is a photodegradation reaction because the degradation process using a photocatalytic semiconductor requires the presence of light. This research was carried out in dark and light conditions to maximize the occurrence of photocatalysts and to ensure that the light of the reactions was a photodegradation reaction. The reason is because when the material is mixed with dyes, adsorption reactions and photodegradation reactions are likely to occur.

4. Conclusions

To conclude, the results of this study have found that higher calcination temperatures can affect the characteristics of the photocatalytic material, including morphology, functional groups, crystal structure, crystal lattice, crystallinity, surface area, pore size, pore volume, and energy band gap. The photocatalytic activity of ZnO and ZnO/Mopl-CTAB to degrade methyl orange was successfully investigated under light and dark conditions. The photocatalytic degradation of methyl orange showed that ZnO/Mopl-CTAB performed better than ZnO under the same test conditions. ZnO/Mopl-CTAB 450 showed the highest methyl orange degradation percentage (78%) in 50 min in light conditions, whereas in dark conditions, 52% methyl orange had been degraded by ZnO/Mopl-CTAB 150 in 40 min. The reaction kinetics in the photodegradation process of MO using ZnO and ZnO/Mopl-CTAB at different calcination temperatures in dark and light conditions used a kinetic model that followed the pseudo-second-order reaction.

Acknowledgment

Gratitude is expressed to the Ministry of Education, Culture, Research, and Technology of the Republic of Indonesia for the funding support for this study in Scheme of Collaborative Research between Universities with Master Contract Number of No. 075/E5/P6.02.00.PT/2022 and Subsidiary Contract Number of No. 014/SP2H/PT-L/LL7/2022 and No. 01/040.1/PN.02.01/L/III/2022. We also would like to thank to Universitas Islam Kadiri and Institut Teknologi Sepuluh Nopember for great supports especially facilities. There are no authors in conflict of interest for any subjects.

CRediT Author Statement

Author Contributions: A.D. Rosanti: Conceptualization, Methodology, Investigation, Resources, Data Curation, Writing, Review and Editing, Supervision, Formal Analysis, Writting Draft Preparation, Visualization, Project Administration; F. Hidayat: Conceptualization, Methodology, Software Investigation, Resources, Data Curation, Writing, Review and Editing; Y. Kusumawati: Conceptualization, Methodology, Investigation, Resources, Validation, Writing, Review and Editing, Data Curation; A. Fadlan: Conceptualization, Methodology, Investigation, Resources, Validation, Writing, Review and Editing, Data Curation. R.A. Shobirin: Software, Writing, Editing. F.K. Wijaya: Investigation, Resources, Data Curation. All authors have read and agreed to the published version of the manuscript.

References

[1] Pratisarawirya, G.L. (2020). Analisis kualitas air akibat limbah tekstil di sungai samin kecamatan mojolaban kabupaten sukoharjo. *Skripsi (Undergraduate Thesis)*. Program Studi Geografi. Universitas Muhammadiyah Surakarta

[2] Raganata, T.C., Aritonang, H., Suryanto, E. (2020). Sintesis Fotokatalis Nanopartikel ZnO untuk Mendegradasi Zat Warna Methylene Blue. *Chemistry Progress*, 12(2), 54–58. DOI: 10.35799/cp.12.2.2019.27923.

[3] Komarawidjaja, W. (2016). Sebaran Limbah Cair Industri Tekstil dan Dampaknya di Beberapa Desa Kecamatan Rancaekek Kabupaten Bandung Outspread of Textile Industry Waste Water and its Impact to a Number of Villages in Rancaekek District, Bandung Regency. *Jurnal Teknologi Lingkungan*, 17(2), 118–125. DOI: 10.29122/jtl.v17i2.1045

[4] Al-Tohamy, R., Ali, S.S., Li, F., Okasha, K.M., Mahmoud, Y.A.G., Elsamahy, T., Jiao, H., Fu, Y., Sun, J. (2022). A critical review on the treatment of dye-containing wastewater: Ecotoxicological and health concerns of textile dyes and possible remediation approaches for environmental safety. *Ecotoxicology and Environmental Safety*, 231, 113160. DOI: 10.1016/j.ecoenv.2021.113160.

[5] Briffa, J., Sinagra, E., Blundell, R. (2020). Heavy metal pollution in the environment and their toxicological effects on humans. *Heliyon*, 6(9), e04691. DOI: 10.1016/j.heliyon.2020.e04691.

[6] Adjid, G.A.F.A., Kurniawan, A., Nazriati, N. (2022). Textile Industry Waste Pollution in the Konto River: A Comparison of Public Perceptions and Water Quality Data. *The Journal of Experimental Life Sciences*, 12(3), 105–116. DOI: 10.21776/ub.jels.2022.012.03.05.

[7] Rosanti, A.D., Kusumawati, Y., Hidayat, F., Fadlan, A., Wardani, A.R.., Anggraeni, H.A. (2022). Adsorption of Methylene Blue and Methyl Orange from Aqueous Solution using Orange Peel and CTAB-Modified Orange Peel. *Journal Of the Turkish Chemical Society Chemistry*, 9(1), 237–246. DOI: https://doi.org/10.18596/jotcsa.1003132.

[8] Rosanti, A.D., Hidayat, F., Kusumawati, Y., Fadlan, A., Wardani, A.R.., Latifah, E.U. (2022). The effect of orange peel waste addition on ZnO characteristics and its ability to degrade methyl orange. In: *IOP Conference Series: Earth and Environmental Science*. pp. 1–8. DOI: 10.1088/1755-1315/1041/1/012008.

[9] Mandar, S., Zainul, R. (2019). Sintesis dan Karakterisasi Nano ZnO doping Cu. *Chemistry Journal*, 8(1), 20–23. DOI: 10.24036/p.v8i1.104122

[10] Nelson, Ngatijo, Nurjanah, S., Maghviroh, N.A., Bemis, R. (2019). Sintesis dan karakterisasi fotokatalis ZnO/karbon aktif dan aplikasinya pada degradasi rhodamin B. *Chempublish Journal*, 4(2), 101–113. DOI: 10.22437/chp.v4i2.7936.

[11] Adeel, M., Saeed, M., Khan, I., Muneer, M., Akram, N. (2021). Synthesis and Characterization of Co-ZnO and Evaluation of Its Photocatalytic Activity for Photodegradation of Methyl Orange. *ACS Omega*, 6(2), 1426–1435. DOI: 10.1021/acsomega.0c05092.

[12] Chen, C., Liu, J., Liu, P., Yu, B. (2011). Investigation of Photocatalytic Degradation of Methyl Orange by Using Nano-Sized ZnO Catalysts. *Advances in Chemical Engineering and Science*, 01(01), 9–14. DOI: 10.4236/aces.2011.11002.

[13] Kumar, R., Kumar, G., Umar, A. (2013). ZnO nano-mushrooms for photocatalytic degradation of methyl orange. *Materials Letters*, 97, 100–103. DOI: 10.1016/j.matlet.2013.01.044.

[14] Zhou, J., Zhang, Z., Kong, X., He, F., Zhao, R., Wu, R., Wei, T., Wang, L., Feng, J. (2020). A novel P-N heterojunction with staggered energy level based on ZnFe2O4 decorating SnS2 nanosheet for efficient photocatalytic degradation. *Applied Surface Science*, 510, 145442. DOI: 10.1016/j.apsusc.2020.145442.

[15] Khan, F., Ansari, S.A., Ahmad, A. (2017). Study of Photocatalytic activity of ZnO and TiO2 nanoparticles. *International Journal of Engineering and Applied Sciences*, 4(11), 130–136.

[16] Mirzaeifard, Z., Shariatinia, Z., Jourshabani, M., Rezaei Darvishi, S.M. (2020). ZnO Photocatalyst Revisited: Effective Photocatalytic Degradation of Emerging Contaminants Using S-Doped ZnO Nanoparticles under Visible Light Radiation. *Industrial and Engineering Chemistry Research*, 59(36), 15894–15911. DOI: 10.1021/acs.iecr.0c03192.

[17] Basit, R.A., Abbasi, Z., Hafeez, M., Ahmad, P., Khan, J., Khandaker, M.U., Al-Mugren, K.S., Khalid, A. (2023). Successive Photocatalytic Degradation of Methylene Blue by ZnO, CuO and ZnO/CuO Synthesized from Coriandrum sativum Plant Extract via Green Synthesis Technique. *Crystals*, 13(2) DOI: 10.3390/cryst13020281.

[18] Majumder, S., Chatterjee, S., Basnet, P., Mukherjee, J. (2020). ZnO based nanomaterials for photocatalytic degradation of aqueous pharmaceutical waste solutions – A contemporary review. *Environmental Nanotechnology, Monitoring and Management*, 14, 100386. DOI: 10.1016/j.enmm.2020.100386.

[19] Zhong, J.B., Li, J.Z., Xiao, Z.H., Hu, W., Zhou, X.B., Zheng, X.W. (2013). Improved photocatalytic performance of ZnO prepared by sol-gel method with the assistance of CTAB. *Materials Letters*, 91, 301–303. DOI: 10.1016/j.matlet.2012.10.040.

[20] Mornani, E.G., Mosayebian, P., Dorranian, D., Behzad, K. (2016). Effect of calcination temperature on the size and optical properties of synthesized ZnO nanoparticles. *Journal of Ovonic Research*, 12(2), 75–80.

[21] Golsheikh, A.M., Kamali, K.Z., Huang, N.M., Zak, A.K. (2018). Effect of calcination temperature on performance of ZnO nanoparticles for dye-sensitized solar cells. *Powder Technology*, 329, 282–287. DOI: 10.1016/j.powtec.2017.11.065.

[22] Gupta, M.K., Tandon, P.K., Shukla, N., Singh, H., Srivastava, S. (2020). Efficient removal of methyl orange and rhodamine-B dyes with low cost banana peel activated carbon. *Asian Journal of Chemistry*, 32(5), 1121–1127. DOI: 10.14233/ajchem.2020.22580.

[23] Krishnakumar, V., Elansezhian, R. (2021). Dispersion stability of zinc oxide nanoparticles in an electroless bath with various surfactants. *Materials Today: Proceedings*, 51, 369–373. DOI: 10.1016/j.matpr.2021.05.467.

[24] Xu, X.L., Chen, Y., Ma, S.Y., Yan, S.H., Mao, Y.Z., Wang, T., Bian, H.Q. (2015). CTAB-assisted synthesis of unique 3D ZnO and the acetone sensing performances. *Materials Letters*, 151, 5–8. DOI: 10.1016/j.matlet.2015.03.017.

[25] Elfeky, S.A., Mahmoud, S.E., Youssef, A.F. (2017). Applications of CTAB modified magnetic nanoparticles for removal of chromium (VI) from contaminated water. *Journal of Advanced Research*, 8(4), 435–443. DOI: 10.1016/j.jare.2017.06.002.

[26] Abdi, M.M., Tahir, P.M., Liyana, R., Javahershenas, R. (2018). A surfactant directed microcrystalline cellulose/polyaniline composite with enhanced electrochemical properties. *Molecules*, 23(10) DOI: 10.3390/molecules23102470.

[27] Bukit, B.F., Frida, E., Humaidi, S., Sinuhaji, P. (2022). Preparation and characterization of CTAB surfactant modified TiO_2 nanoparticles as antibacterial fabric coating material. *Journal of Physics: Conference Series*, 2165(1) DOI: 10.1088/1742-6596/2165/1/012022.

[28] Hanafi, M.F., Sapawe, N. (2019). Effect of Calcination Temperature on the Structure and Catalytic Performance of ZrO_2 Catalyst in Phenol Degradation. *Materials Today: Proceedings*, 19(10), 1533–1536. DOI: 10.1016/j.matpr.2019.11.179.

[29] Purbaningtias, T.E., Kurniawati, P., Wiyantoko, B., Prasetyoko, D., Suprapto, S. (2017). Pengaruh Waktu Aging Pada Modifikasi Pori Zeolit Alam Dengan Ctabr. *JST (Jurnal Sains dan Teknologi)*, 6(2), 321. DOI: 10.23887/jst-undiksha.v6i2.9322.

[30] Lan, K., Zhao, D. (2022). Functional Ordered Mesoporous Materials: Present and Future. *Nano Letters*, 22(8), 3177–3179. DOI: 10.1021/acs.nanolett.2c00902.

[31] Ariga, K., Vinu, A., Yamauchi, Y., Ji, Q., Hill, J.P. (2012). Nanoarchitectonics for mesoporous materials. *Bulletin of the Chemical Society of Japan*, 85(1), 1–32. DOI: 10.1246/bcsj.20110162.

[32] Manga, J., Widiyanti, S.E. (2020). Studi Proses Hidrotermal pada Sintesis Material Mesopori dan Karakteristik Stabilitas Adsorpsi. In: *Prosiding 4th Seminar Nasional Penelitian & Pengabdian Kepada Masyarakat 2020*. pp. 98–102.

[33] Wang, Y.D., Zhang, S., Ma, C.L., Li, H.D. (2007). Synthesis and room temperature photoluminescence of ZnO/CTAB ordered layered nanocomposite with flake-like architecture. *Journal of Luminescence*, 126(2), 661–664. DOI: 10.1016/j.jlumin.2006.10.018.

[34] Ai, F., Zhao, G., Lv, W., Lin, J. (2020). Facile synthesis of cetyltrimethylammonium bromide-loaded mesoporous silica nanoparticles for efficient inhibition of hepatocellular carcinoma cell proliferation. *Materials Research Express*, 7(8), 085008. DOI: 10.1088/2053-1591/abad15.

[35] Campbell, R.A., Parker, S.R.W., Day, J.P.R., Bain, C.D. (2004). External reflection FTIR spectroscopy of the cationic surfactant hexadecyltrimethylammonium bromide (CTAB) on an overflowing cylinder. *Langmuir*, 20(20), 8740–8753. DOI: 10.1021/la048680x.

[36] Duarte, J., Cruz-Lopes, L., Dulyanska, Y., Domingos, I., Ferreira, J., de Lemos, L.T., Esteves, B. (2017). Orange peel liquefaction monitored by FTIR. *Journal of International Scientific Publications: Agriculture & Food*, 5, 309–313.

[37] Feng, N., Guo, X., Liang, S. (2009). Adsorption study of copper (II) by chemically modified orange peel. *Journal of Hazardous Materials*, 164(2–3), 1286–1292. DOI: 10.1016/j.jhazmat.2008.09.096.

[38] Bassim, S., Mageed, A.K., AbdulRazak, A.A., Al-Sheikh, F. (2023). Photodegradation of Methylene Blue with Aid of Green Synthesis of CuO/TiO_2 Nanoparticles from Extract of Citrus Aurantium Juice. *Bulletin of Chemical Reaction Engineering & Catalysis*, 18(1), 1–16. DOI: 10.9767/bcrec.16417.

[39] Sangeetha, A., Jaya Seeli, S., Bhuvana, K.P., Kader, M.A., Nayak, S.K. (2019). Correlation between calcination temperature and optical parameter of zinc oxide (ZnO) nanoparticles. *Journal of Sol-Gel Science and Technology*, 91(2), 261–272. DOI: 10.1007/s10971-019-05000-8.

[40] Wang, Y., Li, Y., Zhou, Z., Zu, X., Deng, Y. (2011). Evolution of the zinc compound nanostructures in zinc acetate single-source solution. *Journal of Nanoparticle Research*, 13(10), 5193–5202. DOI: 10.1007/s11051-011-0504-y.

[41] Laetsch, T., Downs, R.. (2006). Software for identification and refinement of cell parameters from powder diffraction data of minerals using the RUFF Project and American mineralogist crystal structure databases. Abstracts from the *19th General Meeting of the International Mineralogical Association*. 23-28.

[42] Kowalik, P., Konkol, M., Antoniak-Jurak, K., Próchniak, W., Wiercioch, P., Rawski, M., Borowiecki, T. (2015). Structure and morphology transformation of ZnO by carbonation and thermal treatment. *Materials Research Bulletin*, 65, 149–156. DOI: 10.1016/j.materresbull.2015.01.032.

[43] Cullity, B.D. (1994). *Elements of diffraction-quasi-optics*. Second Edition. London. Addison-Wesley Publishing Company Inc.

[44] Aziz, S.B., Marf, A.S., Dannoun, E.M.A., Brza, M.A., Abdullah, R. (2020). The Study of the Degree of Crystallinity, Electrical Equivalent Circuit, and Dielectric Properties of Polyvinyl Alcohol (PVA)-Based Biopolymer Electrolytes Shujahadeen. *Polymers*, 12(10), 2184. DOI: 10.3390/polym12102184.

[45] Momma, K., Izumi, F. (2008). VESTA: A three-dimensional visualization system for electronic and structural analysis. *Journal of Applied Crystallography*, 41(3), 653–658. DOI: 10.1107/S0021889808012016.

[46] Saleem, M., Fang, L., Ruan, H., Wu, F., Huang, Q., Xu, C., Kong, C. (2012). Effect of zinc acetate concentration on the structural and optical properties of ZnO thin films deposited by Sol-Gel method. *International Journal of the Physical Sciences*, 7(23), 2971–2979. DOI: 10.5897/ijps12.219.

[47] Kibasomba, P.M., Dhlamini, S., Maaza, M., Liu, C.P., Rashad, M.M., Rayan, D.A., Mwakikunga, B.W. (2018). Strain and grain size of TiO_2 nanoparticles from TEM, Raman spectroscopy and XRD: The revisiting of the Williamson-Hall plot method. *Results in Physics*, 9, 628–635. DOI: 10.1016/j.rinp.2018.03.008.

[48] Mir, F.A. (2014). Transparent wide band gap crystals follow indirect allowed transition and bipolaron hopping mechanism. *Results in Physics*, 4, 103–104. DOI: 10.1016/j.rinp.2014.06.001.